TEM STUDY OF LIME SILICATES IN Y-81020 PRIMITIVE CHONDRITE. M. Komatsu[1], T. J. Fagan[2], and T. Mikouchi[3], [1]Waseda Institute for Advanced Study, Waseda Univerity, 1-6-1, Shinjuku, Tokyo, Japan (komatsu@aoni.waseda.jp), [2]Department of Earth Sciences, Waseda University, [3]Department of Earth and Planetary Science, Graduate School of Science, University of Tokyo.

Introduction: Low-iron, Mn-enriched (LIME) silicates are important components in the primitive solar system materials; they have been identified in IDPs [1], chondrules and matrices of primitive chondrites [2, 3], and in Wild 2 cometary grains [4]. LIME olivine has also been observed in some amoeboid olivine aggregates (AOAs) in primitive chondrites [5, 6]. Mineralogy and chemical compositions of AOAs are similar to those predicted by equilibrium thermodynamic condensation models [e.g., 7], suggesting that AOAs formed primarily by gas-solid condensation at low oxygen fugacities [8].

In this study, we combine standard thin section petrography with FIB/TEM scale observations to examine variations in Mn concentrations and distribution patterns in AOAs from the CO3 chondrite Y-81020. Y-81020 is one of the most primitive chondrites, so it can be used to study components of chondrites that formed in the solar nebula and have undergone minimal subsequent alteration.

Methods: One polished thin section of Y-81020 was studied. After SEM and EPMA analyses, TEM sections were prepared from two AOAs (#1 and #18) and 1 chondrule (#62) using FIB techniques. TEM images and EDS spectra were collected using a JEOL JEM-2100F FE-TEM equipped with JED 2300T EDX system at Waseda University.

Results and Discussions:

1. Distribution of Mn in Y-81020 AOAs

Most AOAs in Y-81020 are composed of nodules having anorthite ±spinel cores, Al-diopside-rich mantles and closely (compact) or loosely (porous) packed forsterite rims. Olivine Mn contents and distribution patterns vary between different AOAs (Fig. 1). Compact AOAs tend to have limited Mn enrichment (in their rims, e.g., AOA#61), or no Mn-enrichment (e.g., AOA#60, Fig. 1). In contrast, porous AOAs tend to have higher Mn content both in core and rim (see [9] and AOA#18, Fig. 1). Y-81020 AOAs show little evidence of alteration to alkali- or FeO-rich minerals.

2. Mn-enriched olivine and pyroxene

Some AOAs in Y-81020 contain low-Ca pyroxene. Low-Ca pyroxene is found in AOAs from most primitive carbonaceous chondrites [10,11]. Our analyses show that the compositions of olivine and pyroxene mimic each other: if olivine is LIME, then the coexisting pyroxene is also LIME.

3. Low-Mn, normal AOA#1

The boundary between pyroxene and forsterite is unclear under BSE images, but can be identified in EDS elemental maps of Ca, Si and Mg (Fig. 2). There is no change in Mn content between olivine and low-Ca pyroxene in our FIB slice of AOA#1(Fig. 2d).

4. LIME AOA #18

In AOA#18, Mn-enrichment in olivine toward the rim of AOA occurs (Fig. 1). It is likely that the enrichment of Mn in the rim of AOA#18 reflects condensation of Mn-enriched olivine with decreasing temperature, which is supported by the condensation models by [12] and [13]. In addition, AOAs may have experienced sintering which resulted in the distinct Mn zoning in compact AOAs after aggregation [9]. In any case, the duration of heating during condensation and subsequent thermal events were insufficient to homogenize Mn-concentrations in AOA#18 olivines.

Based on the TEM-EDS observation, there may be weak enrichment in Mn toward the rim (Fig. 3c; left side is close to the rim of AOA#18), but it is difficult to determine. In addition to Mn-enriched silicates, submicron sized Fe-Ni metal grains are observed. The metal grains show distinctive Ni zoning (Fig. 3e). Zoning of Ni content in metal grains is predicted in condensation and diffusion calculations [14].

5. LIME chondrule #62

CHD#62 is a ~30 μm sized spherical chondrule. It is mainly composed of low-Ca pyroxene which contains up to 2.5 wt.% of MnO. We performed TEM analysis of a FIB section from the core of this chondrule. The FIB section contains a small amount of anorthite (~100 nm), and mesostatis enclosed within submicron sized Mn-enriched enstatite (Fig. 4). Mesostasis is amorphous or poorly crystallized (Fig. 4d).

Mn-rich pyroxenes are also observed in a chondrule in Allende [3]. They are present only in the thick rim around the chondrule and contain ~4 wt.% of MnO, but also contain up to ~9 wt.% FeO. Allende experienced a higher degree of alteration than Y-81020, and FeO content in silicates is higher than less altered CV chondrites. It is possible that the Mn-rich chondrule rim of [3] has a mixed origin, with Mn-enrichment from a nebular process and high FeO due to parent body alteration.

Conclusion: Our recent study [11] shows that Mn-rich olivine is commonly observed in AOAs from weakly metamorphosed Kaba and Y-86009 (CVs). On the other hand, AOAs in metamorphosed type 3 carbo-

naceous chondrites lack LIME silicates. With increasing petrologic sub-types, FeO increases and MnO decreases in AOA olivine [11].

The present study shows that: (1) Mn-concentrations in AOA olivine and low-Ca pyroxene are correlatated at the FIB/TEM scale; and (2) Ni-zoning occurs in AOA metal grains, indicating lack of equilibration during condensation. Furthermore, the presence of glass in chondrule #62 confirms the primitive nature of Y-81020. MnO vs. FeO concentrations in AOA olivines can be sensitive indicators of both condensation and alteration conditions.

References: [1] Klöck W. et al. (1989) *Nature*, 339, 126-128. [2] Ichikawa O. and Ikeda Y. (1995) *Proc. of NIPR Symp., 8*, 63-78. [3] Rubin A. (1984) *American Mineral.*, 69, 880-888. [4] Zolensky M. E. et al. (2006) *Science*, *314*, 1735-1753. [5] Weisberg M. K. et al. (2004) *MaPS, 39*, 1741-1753. [6] Sugiura N. et al. (2009) *MaPS, 44*, 559-572. [7] Yoneda S. and Grossman L. (1995) *GCA, 59*, 3413-3444. [8] Krot A. N. et al. (2005) *GCA, 69*, 1973-1881. [9] Krot A. N. et al. (2004) *Chemie der Erde*, *64*, 185-239. [11] Komatsu M. et al. (2013) *LPS XLIV*, Abstract #1847. [12] Ebel D. S. et al. (2012) *MaPS., 47*, 585-593. [13] Petaev M. et al. (2005) *MaPS , 40*, suppl., #5247. [14] Petaev M. et al. (2003) *GCA, 67*, 1737-1751.

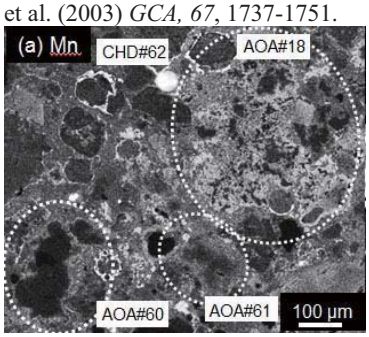

Fig.1. X-ray elemental maps of porous and compact AOAs in Y-81020.

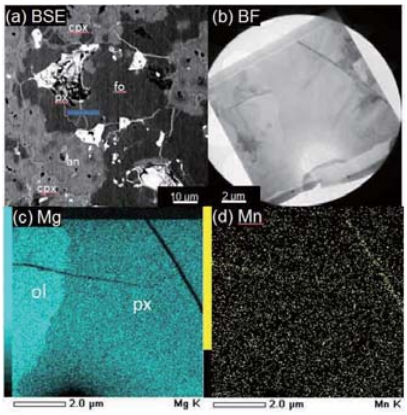

Fig.2. BSE (a), low-magnification TEM image (b), and X-ray elemental maps (c, d) of compact AOA #1 in Y-81020. A clear boundary is observed in Mg, but not in Mn.

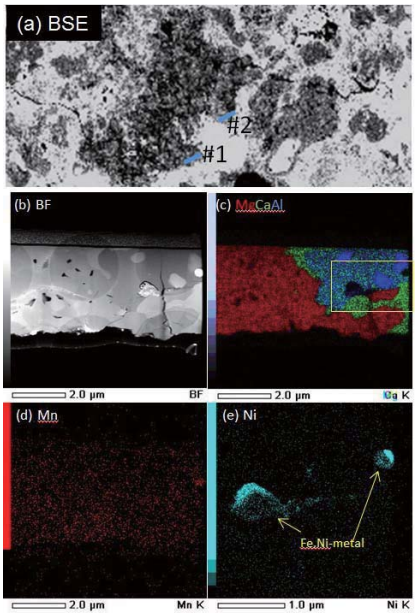

Fig.3. (a) BSE image of AOA #18. TEM sections are taken from the rim of the AOA (shown in blue line). (b) low-magnification TEM image of FIB section #2. (c, d) Combined X-ray elemental map (R=Mg, G=Ca, B=Al), and Mn elemental map of FIB section. (e) X-ray elemental map of Ni of the outlined area in (c).

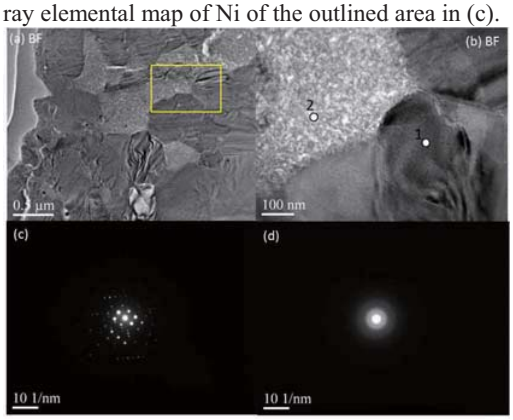

Fig. 4. (a, b) low-magnification TEM images of chondrule #62. (c) SAED pattern of low-Ca pyroxene (c) and amorphous phase (d) (#1 and #2 in (b), respectively).